MOLECULAR AND CELLULAR BIOLOGY, Jan. 2007, p. 44–53 Vol. 27, No. 1
0270-7306/07/$08.00+0 doi:10.1128/MCB.01824-06

"Skittish" *Abca2* Knockout Mice Display Tremor, Hyperactivity, and Abnormal Myelin Ultrastructure in the Central Nervous System▽†

Jody T. Mack,[1] Vladimir Beljanski,[1] Athena M. Soulika,[2] Danyelle M. Townsend,[3] Carol B. Brown,[1] Warren Davis,[1] and Kenneth D. Tew[1]*

Department of Cell and Molecular Pharmacology and Experimental Therapeutics, Medical University of South Carolina, 173 Ashley Avenue, P.O. Box 250505, Charleston, South Carolina 29425[1]; Department of Neurology, University of California Davis School of Medicine, and Shriners Hospitals for Children—Northern California, 2425 Stockton Boulevard, Sacramento, California 95817[2]; and Department of Pharmaceutical Sciences, Medical University of South Carolina, 280 Calhoun Street, Charleston, South Carolina 29425[3]

Received 26 September 2006/Accepted 12 October 2006

The ATP-binding cassette transporter 2 (ABCA2) is an endolysosomal protein most highly expressed in the central and peripheral nervous system tissues and macrophages. Previous studies indicated its role in cholesterol/steroid (estramustine, estradiol, and progesterone) trafficking/sequestration, oxidative stress response, and Alzheimer's disease. Developmental studies have shown its expression during macrophage and oligodendrocyte differentiation, processes requiring membrane growth. To determine the in vivo function(s) of this transporter, we generated a knockout mouse from a gene-targeted disruption of the murine ABCA2 gene. Knockout males and females are viable and fertile. However, a non-Mendelian inheritance pattern was shown among male progeny of heterozygous crosses. Compared to wild-type and heterozygous littermates, knockout mice displayed a tremor without ataxia, hyperactivity, and reduced body weight; the latter two phenotypes were more marked in females than in males. This sexual disparity suggests a role for ABCA2 in hormone-dependent neurological and/or developmental pathways. Myelin sheath thickness in the spinal cords of knockout mice was greatly increased compared to that in wild-type mice, while a significant reduction in myelin membrane periodicity (compaction) was observed in both spinal cords and cerebra of knockout mice. Loss of ABCA2 function in vivo resulted in abnormal myelin compaction in spinal cord and cerebrum, an ultrastructural defect that we propose to be the cause of the phenotypic tremor.

ATP-binding cassette transporter 2 (ABCA2) is the largest of the 48 known members of the ABC transporter superfamily (7). Many ABC transporters contribute to drug resistance phenotypes and/or human disease etiologies (7). Previous studies have provided evidence for a link between ABCA2 expression/function and cholesterol homeostasis (6, 19), oxidative stress response (5), and resistance to estrogen-based therapeutics (estradiol, estramustine, and progesterone) (1, 16, 18, 23, 41). This protein is localized primarily at the endolysosomal membrane (41). In vivo, expression of ABCA2 has been illustrated in cells and tissues requiring high levels of cholesterol (for generation of cellular membrane) and/or steroid hormones. These include myelinating cells of the central nervous system (CNS) and peripheral nervous system oligodendrocytes and Schwann cells, respectively (20, 48), excitatory and inhibitory neurons (GABAergic and glutamatergic) (2), reproductive tissues (prostate, ovary, and uterus) (18), macrophages (5, 19, 48), and T-cell acute lymphoblastic leukemia (9) and human vestibular schwannomas (42). Putative transcription factor binding sites in the promoter of this transporter are associated with differentiation in neural and myeloid tissues (19). Further studies have confirmed this observation, as ABCA2 expression was shown to be developmentally up-regulated in day 14 p.c. embryos in concert with myelin sheath-associated proteins (38, 41, 47) and in monocytes during differentiation into macrophages (19).

Oxidative stress, a natural phenomenon occurring in development, differentiation, and aging, stimulates the generation of lipid hydroperoxides from cell membrane phospholipids. Long-term oxidative damage in brain tissue is a hallmark of Alzheimer's disease (AD) pathology (15). AD predisposition is associated, albeit controversially, with circulating and cerebrospinal fluid (CSF) cholesterol levels and linkage to cholesterol homeostasis genes, including the APOE e4, CYP46A1, and ABCA1 genes (40). Recently, a single-nucleotide polymorphism within exon 14 of *Abca2* (rs908832) was linked to early-onset AD (26, 43). This mutation produces elevated cholesterol levels in CSF, a risk factor for AD (43). The effects on CSF cholesterol and AD age of onset are shared by mutants of *Abca1*, the closest relative of *Abca2*; both are cholesterol-responsive genes with identity in a C-terminal region (VFVNFA) associated with the ABCA1-apoA1 interaction and lipid efflux (11, 19). Further, ABCA2 is expressed in regions of the brain associated with adult neurogenesis and AD pathology (the temporal, frontal, and subventricular zones and the dentate gyrus) (2, 5). Ectopic expression has elicited differential expression of oxidative stress response genes and resistance upon exposure to free radicals (5). In addition, the

* Corresponding author. Mailing address: Department of Cell and Molecular Pharmacology and Experimental Therapeutics, Medical University of South Carolina, 173 Ashley Avenue, P.O. Box 250505, Charleston, SC 29425. Phone: (843) 792-2514. Fax: (843) 792-2475. E-mail: tewk@musc.edu.

† Supplemental material for this article may be found at http://mcb.asm.org/.

▽ Published ahead of print on 23 October 2006.

TABLE 1. Primers for RT- and real-time PCR

Gene	Forward primer	Reverse primer	Product (bp)
Abca2	CTCACTGGTGCAGACGTTGT	TTCAGAATGAGGTCCCAGATG	150
Abca1	AGCCAGAAGGGAGTGTCAGA	CATGCCATCTCGGTAAACCT	102
Abca3	TGCTCATGCTGAGTTTCACC	GACACAGAACAGGAGCGTCA	191
Abca5	TGGTAGCCGCAAGTCTTTCT	CGATGCCTGCAGAACTGTAA	194
Abca7	ATCCTAGTGGCTGTCCGTCA	ATGGCTTGTTTGGAAAGTGG	70
MBP	AGTACCTGGCCACAGCAAGT	AGGATGCCCGTGTCTCTGT	76
CNP	CATCCTCAGGAGCAAAGGAG	TGAATAGCGTCTTGCACTCG	96
PLP	GAGGCCAACATCAAGCTCAT	CAAACTTGTCGGGATGTCCT	78
NPC1	AGCGCCATTTACCATCATTC	CCTTTGGTGGCATTTCTCAT	78
GAPDH	GTGGACCTCATGGCCTACAT	GCCTCTCTTGCTCAGTGTCC	83

transporter was shown to colocalize with the amyloid precursor protein and amyloid β peptide (5), both of which are associated with senile plaque formation and AD progression (36). Taken together, these reports suggest a functional link between ABCA2 and AD pathology.

In order to elucidate the in vivo functions of this transporter, we report the generation and characterization of an *Abca2* knockout (KO) mouse that displayed an obvious tremor and abnormal myelin sheath ultrastructure in spinal cord and cerebrum. Reduced body size and hyperactivity were two phenotypes observed in KO animals, but these were most prominent in female mice. The data suggest a sex-dependent disparity in the response to ABCA2 loss of function, an observation that may help uncover the link connecting this transporter and steroid hormones with neurological disease.

MATERIALS AND METHODS

Generation of *Abca2* knockout by homologous recombination. A targeting construct, containing two arms of homology (1.5 kb and 5.5 kb), enabled the homologous recombination and disruption of the murine ABCA2 gene with a neomycin resistance cassette, replacing exons 24 to 30. This region corresponds to the first nucleotide-binding domain (NBD1) of the transporter. Gene-targeted *Abca2* knockout mouse embryonic stem (ES) cells from the mouse strain 129/Sv were grown in selective media (G418 and ganciclovir). ES clones were screened by Southern analysis of an XmnI restriction digest of PCR products (generated using forward and reverse primers 5′TTCCAGGCGTGATCTTCCAGACACG GAAGGA3′ and 5′CGCTTCACCAGGAGCCCATGGAACTG3′). Digests were visualized using a ^{32}P-labeled 5′ probe where nontargeted or gene-targeted clones revealed 7,046-bp or 4,155-bp bands, respectively. Targeted clones were utilized for microinjection into C57BL6/J blastocysts, conducted at the Medical University of South Carolina (MUSC) Gene Targeting & Knockout Mouse Facility. Breeding of $Abca2^{-/-} \times Abca2^{-/-}$ mice has resulted in the birth of viable offspring, confirming the fertility of *Abca2* knockout mice. Animals were housed in microisolation cages and provided with standard rodent chow and tap water ad libitum. Animal experiments were conducted in accordance with the MUSC Institutional Animal Care and Use Committee.

Genotypic analysis and TaqMan PCR. DNA was isolated from tail biopsy samples in a buffer containing 10 mM Tris-HCl (pH 8.3), 50 mM KCl, 2.5 mM $MgCl_2$-$6H_2O$, 0.45% Nonidet-P40, 0.45% Tween-20, and 33 μg/ml proteinase K, followed by 16 h of incubation at 55°C. DNA was isolated from supernatant following centrifugation (8,000 × *g*; 5 min), and proteinase K was denatured by 10 min of incubation at 99°C. Genotypes of +/+ (wild type [WT]), +/− (heterozygous [HET]), and −/− (KO) mice were determined by using PCR to amplify a 219-bp genomic region flanking wild-type *Abca2* exon 28 (forward: 5′CTTCTGCTCCCCCTTCCTT3′; reverse: 5′CCCCACACACCTGAAAGAG 3′). The gene-targeted KO allele, containing the neomycin resistance gene (*neo*), was amplified to generate a 364-bp product (forward, 5′TGCTCCTGCCGAG AAAGTAT3′; reverse, 5′AATATCACGGGTAGCCAACG3′). PCR cycles were conducted with 2.5× MasterMix (Eppendorf, Hamburg, Germany) as follows: 3 min at 95°C followed by 25 cycles of 15 s at 95°C, 30 s at 58°C, and 60 s at 72°C.

Genotypes were further confirmed using a TaqMan PCR (iCycler; Bio-Rad, Hercules, CA) strategy for genomic DNA (five mice per genotype). The primers listed above for *Abca2* exon 28 were used with the probe 5′-6-FAM-CCCAGC GAGGCCGTCAAGAA-3′BHQ1. For a loading control, the glyceraldehyde-3-phosphate dehydrogenase (GAPDH) gene was also analyzed using the forward and reverse primers 5′AAGGGCTCATGACCACAGTC3′ and 5′GTGAGCTT CCCATTCAGCTC3′ and the probe 5′-6-FAM-ATGATGGCTGTGGGGCTG CC-3′BHQ1. TaqMan PCR cycles were conducted as follows: 3 min at 95°C followed by 40 cycles of 10 s at 55°C and 30 s at 95°C. The mean wild-type cycle threshold C_T values for ABCA2 and GAPDH were used for calibration, and relative levels of genomic ABCA2 were determined for each genotype using the formula $2^{-\Delta\Delta CT}$, as described previously (6).

Real-time and RT-PCR. Total RNA isolated from KO and WT tissue was analyzed by reverse transcription (RT)- and real-time PCR. Extraction of RNA was accomplished using the Nucleospin II kit (Clontech Laboratories, Inc. Mountain View, CA) per the manufacturer's instructions. Three micrograms of total RNA was used to generate cDNA using SuperScript III reverse transcriptase and random hexamer primers according to the protocol provided by the manufacturer (Invitrogen, Carlsbad, CA). To avoid degradation of RNA, reverse transcription was conducted immediately after RNA extraction. The cDNA products were stored at −20°C until analysis by standard PCR and real-time PCR. Primers were designed with the assistance of software provided by the Primer3 website (33) and the Mfold web server (49), allowing the exclusion of template regions containing secondary structures at 55 to 60°C. PCR was conducted using 2.5× MasterMix (Eppendorf) with cDNA template to screen for differences in gene expression and to confirm the expected product sizes (Table 1) versus GAPDH as a loading control. For *Abca2*, primers were specific to exon 26 (Table 1). Real-time PCR was used to calculate the relative expression of genes listed in Table 1 for cerebrum, cerebellum, and spinal cord cDNA using the formula $2^{-\Delta\Delta CT}$ as described previously (6) (SYBR green Supermix and iCycler; Bio-Rad). GAPDH was used as a loading control, and WT expression values were used as the calibrator. Analyses were performed in triplicate for a minimum of 10 mice per genotype.

TEM. Transmission electron microscopy (TEM) images were examined for the effects of ABCA2 loss of function on the ultrastructure of CNS tissue. Animals (three mice per genotype) were anesthetized with 2-2-2 tribromoethanol, administered intraperitoneally, followed by perfusion with 0.1 mM sodium cacodylate and 2% glutaraldehyde (pH 7.3). Cerebrum, cerebellum, and spinal cord were excised, minced, and postfixed in the same fixative used for perfusion. Tissue was processed, embedded in plastic resin, and subjected to transmission electron microscopy (JEOL JEM1210 microscope) at the MUSC Electron Microscopy Facility. Radial thickness of myelin sheath was measured from images taken at magnifications of ×25,000 and ×80,000 using Image J 1.34s software (National Institutes of Health). Periodicity was determined by the average number of major dense lines per micrometer. Measurements were taken from individual axons (a minimum of 75 per tissue) from 20 images (10 at each magnification) per section.

Histology and pathology. For histological examination of tissues, 6-week-old animals (two per sex, four per genotype) were anesthetized as described above and sacrificed by cervical dislocation. Tissues were excised and fixed overnight in 4% paraformaldehyde-phosphate-buffered saline (PBS) (pH 7.4). For bone marrow isolation, both femurs were flushed with PBS using a 20-gauge needle (B-D Biosciences, San Jose, CA) and fixed in between tissue cassette sponges in 4% paraformaldehyde-PBS. All tissues including brain, spinal cord, sciatic nerve, heart, lung, liver, kidney, spleen, bone marrow, gastrointestinal tract, bladder, uterus, ovary, and prostate were embedded in paraffin, sectioned, and stained (hematoxylin and eosin and/or luxol fast blue [LFB]) at the Tissue Procurement Core Facility. Hematoxylin and eosin- and LFB-stained sections were examined

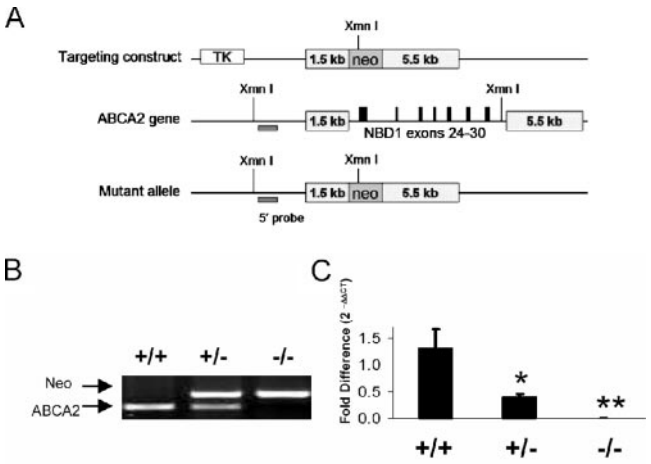

FIG. 1. Gene-targeted disruption of NBD1 of ABCA2. (A) Strategy for the homologous recombination of the targeting construct, containing two arms of homology with the wild-type *Abca2* gene (1.5 kb and 5.5 kb) flanking exons 24 to 30 (coding for NBD1). Successful gene targeting was determined by screening ES cell clones by XmnI digestion and Southern blot analysis (data not shown). (B) Mouse genotypes were determined via PCR analysis of tail biopsy DNA using primers for the neomycin cassette (Neo) and exon 28 of wild-type *Abca2*. (C) Genotypes were further confirmed using a TaqMan PCR strategy (five mice per genotype). The ABCA2 DNA sequence was significantly reduced in HET animals (*, $P = 0.01$) and undetectable in KO (**, $P < 0.0001$). The fold difference in genomic ABCA2 was calculated using the formula $2^{-\Delta\Delta CT}$ as described previously, using GAPDH as a loading control (6). TK, thymidine kinase.

for histopathological differences at the MUSC Department of Pathology and Laboratory Medicine. Further analysis of tissues in a small sample size (two samples each from KO and WT mice) was conducted at the Rodent Histopathology Core Facility at Harvard Medical School.

Western blot analysis. For ABCA2 Western blots, 1 ml of lysis buffer containing 10% glycerol, 1% Triton X-100, and 1 × complete protease inhibitor (Roche, Indianapolis, IN) was added to 50 mg of tissue, followed by homogenization using a glass Dounce homogenizer (20 strokes of a loose-fitting pestle and 20 strokes of a tight-fitting pestle at 4°C). After centrifugation at 3,000 × *g* for 10 min at 4°C, total protein was quantified using the Bio-Rad (Hercules, CA) protein assay reagent. One hundred micrograms of total protein was subjected to 6% sodium dodecyl sulfate-polyacrylamide gel electrophoresis as described previously (41). Primary and secondary antibodies were used at the following dilutions: for ABCA2, 1:500 rabbit polyclonal, for GAPDH, 1:1,000 rabbit polyclonal (Abcam, Cambridge, MA), and for horseradish peroxidase-linked anti-rabbit immunoglobulin G (1:1,000; Amersham Biosciences, Piscataway, NJ). Blots were developed with enhanced chemiluminescence reagents (Bio-Rad) and exposed to autoradiography film (Kodak, New Haven, CT). Densitometry was conducted using Image J 1.34s software (National Institutes of Health) using GAPDH as a loading control for a minimum of 10 mice per genotype.

Rotarod performance. Ability to maintain balance and movement agility on a rotating rod apparatus (rotarod) was assessed for each genotype in 4-, 8-, and 15-week-old mice (five mice per age group) to test changes in performance as described previously (22). Animals were first acclimated to the apparatus by placing them on the lowest speed (4 rpm) for 10 s on each of 3 consecutive days. On day 4, animals were placed on an accelerating rotarod (4 to 40 rpm); the average time to fall (latency), from three trials, was recorded in seconds.

Locomotor assays. Following 3 days of habituation in the testing room, WT and KO animals (8 to 14 weeks of age; 12 mice per genotype) were tested for locomotor activity in Plexiglas activity chambers (22 by 43 by 33 cm^3). These chambers were interfaced to a Digiscan monitor for recording and analysis using VersaMax software (Omnitech Electronics, Columbus, OH). Locomotor activity was recorded in 5-min bins over a 60-min period. Total distance traveled (horizontal activity) and total vertical movement (rearing behavior) were recorded.

Plasma cholesterol measurements. For each animal, 200 μl of whole blood drawn from the submandibular site using a sterile 5-mm lancet (GoldenRod; MEDIpoint, Inc., Mineola, NY) and collected into EDTA-coated tubes (B-D Biosciences, Franklin Lakes, NJ). Blood was centrifuged in the collection tubes at 5,000 × *g* for 15 min to separate plasma. Cholesterol levels (total, free, and esterified) were determined enzymatically per the protocol and standards provided by the manufacturer (Wako Diagnostics, Richmond, VA) for WT, HET, and KO mice 7 weeks of age (four mice per genotype). Colorimetric determination was conducted using a Benchmark plate reader (Bio-Rad) for total, free, esterified, and high-density lipoprotein (HDL) cholesterol per the manufacturer's instructions.

Lipidomics. Lipid composition of CNS tissues was determined at the MUSC Lipidomics Core Facility. Ceramide (C14, C16, C18, C18:1, C20, C24, C24:1, DHC16), sphingosine (Sph, DHSph, Sph-1P), and sphingomyelin (C14-SM, C16-SM, C18-SM, C18:1-SM, C20-SM, C20:1-SM, C22-SM, C22:1-SM C24-SM, C24:1-SM, Lyso-SM) species were analyzed using liquid chromatography/mass spectrometry methodology. Lipids were extracted from tissues (four mice per genotype), and species were quantified in picomoles and normalized to protein concentration as determined using a Bradford assay (Bio-Rad).

Statistics. Statistical significance was determined by chi-square analysis, Student's t testing, or analysis of variance between groups using the online calculator available at http://www.physics.csbsju.edu/stats/. Data are represented as averages of the mean ± standard errors, unless noted otherwise. The variation between groups was considered significant if the *P* value was less than 0.05.

RESULTS

Gene-targeted disruption of NBD1 of ABCA2. A targeting construct, containing two arms of homology (1.5 kb and 5.5 kb), enabled the homologous recombination and disruption of the murine ABCA2 gene with a neomycin resistance cassette, replacing exons 24 to 30 (Fig. 1A). This region corresponds to NBD1 of the transporter. Gene-targeted ES cells were screened by Southern analysis of an XmnI restriction digest of genomic DNA using a ^{32}P-labeled 5′ probe (data not shown). Inheritance of the *Abca2* allele deviates from the expected Mendelian ratio for progeny of HET × HET crosses (Table 2) ($P = 0.008$; chi-square analysis). A lower-than-expected frequency of KO mice is derived from this cross; this deviation occurs in male ($P = 0.009$) but not female ($P = 0.39$) progeny, indicating lethality among male embryos. Breeding of KO × KO mice resulted in viable offspring, confirming the fertility of both sexes. The *Abca2* null genotype does not appear to influence overall survival up to 16 months of age (eldest KO mice from F_1 generation parents).

Disruption of *Abca2* allele confirmed. Genotypes of WT, HET, and KO mice were confirmed using PCR analysis for *Abca2* (Fig. 1B), where the presence of the *neo* cassette and the absence of WT *Abca2* exon 28 indicate the *Abca2* KO genotype. Further analysis by TaqMan PCR showed that HET mice have approximately half the relative level of genomic ABCA2 that WT mice do ($P = 0.01$), and KO mice have levels that are

TABLE 2. Inheritance of the *Abca2* null allele

Cross	Genotype	No. of mice with indicated genotype			Expected male/female ratio	χ^2 analysis result (*P*)
		Female	Male	Total		
WT × chimera	WT	11	21	32	1	0.13
	HET	11	10	21	1	0.13
HET × WT	WT	12	16	28	1	0.52
	HET	15	18	33	1	0.52
HET × HET	WT	58	57	115	1	0.008
	HET	111	106	217	2	0.008
	KO	45	30	75	1	0.008

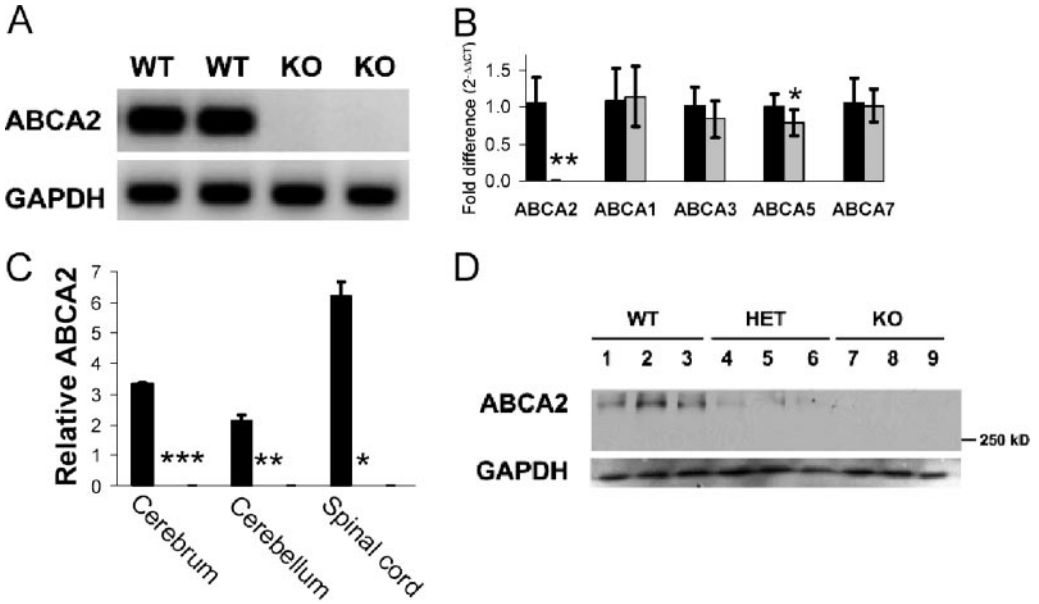

FIG. 2. KO mice lack ABCA2 transcript and protein expression. (A) Representaive RT-PCR products from cerebral cDNA using primers for exon 26. No detectable ABCA2 transcript is present in total RNA collected from cerebrum, cerebellum, or spinal cord samples from KO mice. Similar levels were shown for primers amplifying several regions of the N terminus and the disrupted region (exons 24 to 30) of ABCA2 mRNA (data not shown). (B) Real-time PCR analyses were conducted for selected ABCA subfamily members in cerebellum, and relative levels were calculated (using the formula $2^{-\Delta\Delta CT}$ with GAPDH as a loading control for each sample). We confirmed the lack of expression in KO animals (gray bars) compared to WT animals (black bars) (**, $P < 0.0001$) and also observed slightly lower ABCA5 (*, $P = 0.02$) in KO cerebellum. ABCA1, ABCA3, and ABCA7 levels were similar (P values were 0.67, 0.16, and 0.78, respectively [four mice per genotype]). ABCA1 mRNA in cerebrum was also comparable for WT and KO mice ($P = 0.5$) (data not shown) (nine mice per genotype), making transcriptional compensation in brain tissue unlikely. (C) Densitometry of immunoblots for cerebrum, cerebellum, and spinal cord confirms the absence of protein expression in knockout mouse brain (0 ± 0 for all KO tissues; *, P values were <0.0002, 0.002, and 0.03 compared to WT for cerebrum, cerebellum, and spinal cord, respectively). Relative levels of protein extracts collected from WT ($n = 14$) and KO ($n = 12$) animals are shown. (D) A representative immunoblot probed with a polyclonal rabbit anti-human ABCA2 antibody that cross-reacts with the 270.5-kDa mouse protein indicates high, intermediate, and undetectable levels in cerebrum samples from WT, HET, and KO mice, respectively. Levels of ABCA2 protein were normalized to GAPDH expression.

below detection ($P < 0.0001$) (Fig. 1C). In order to alleviate the concerns associated with comparing mixed background animals to purebred wild-type C57Bl6/J, only littermates of HET × HET crosses were used for comparison.

Loss of global ABCA2 expression in KO mice. Total loss of ABCA2 mRNA and protein occurs in KO mice for all tissues assayed (cerebrum, cerebellum, spinal cord, heart, lung, kidney, liver, spleen, thymus, uterus, prostate, and ovary). ABCA2 transcript was undetectable by RT- and real-time PCR (Fig. 2A and B) ($P < 0.0001$) in exon 26 and for several regions upstream of the disrupting *neo* cassette (1,200 to 1,600 bp, 1,600 to 2,000 bp, 2,701 to 2,880 bp [data not shown]). KO mice are devoid of ABCA2 protein in cerebrum, cerebellum, and spinal cord as determined by Western blot analysis (Fig. 2C and D). CNS tissues from HET mice showed approximately 25 to 50% of WT protein levels (Fig. 2D). These data show the complete ablation of ABCA2 expression at the mRNA and protein level. Thus, animals homozygous for the targeted allele (KO) are functionally null for ABCA2.

Potential compensatory expression of other ABCA transporters in KO tissues was examined by real-time PCR. Similar levels of ABCA1, ABCA3, ABCA5, and ABCA7 transcripts were observed in cerebrum (Fig. 2B) with the exception of a slight but statistically significant decrease in ABCA5 transcript ($P = 0.02$). Liver ABCA1 expression was also similar for both genotypes. We conclude that transcriptional regulation of these A subfamily transporter genes is unaffected in the absence of ABCA2.

Shaking and "skittish" phenotype of *Abca2* KO mice. A distinct shaking phenotype was observed in all *Abca2* KO mice ($n = 100$). Animals tested on a balance beam or held by the tail displayed tremors of the front and hind limbs as well as abrupt, undulating movements down the spine (see the supplemental material). Similar phenotypes were observed in both sexes. When walking in a microisolation cage, KO mice are observed to display a distinct shaking motion of the ears, tail, and body, in contrast to WT mice in the same environment, and increased movement about the cage and climbing behavior on the wire cage top. Animals were often more difficult to catch by the tail than WT littermates and appeared more startled by sound and more frightened of the handler; hence, we designate this mouse line "skittish." Marked tremors of the limbs were observed in animals being held by the tail (see videos S1a and S1b in the supplemental material). However, KO animals showed no significant increase in ataxia as measured by the number of front or hind limb slips that individual mice displayed after placement on a 1-cm-diameter metal balance beam. However, we did observe impairment in the ability of the KO mice to counterbalance their weight on four paws when placed perpendicular to the beam and a proclivity to move

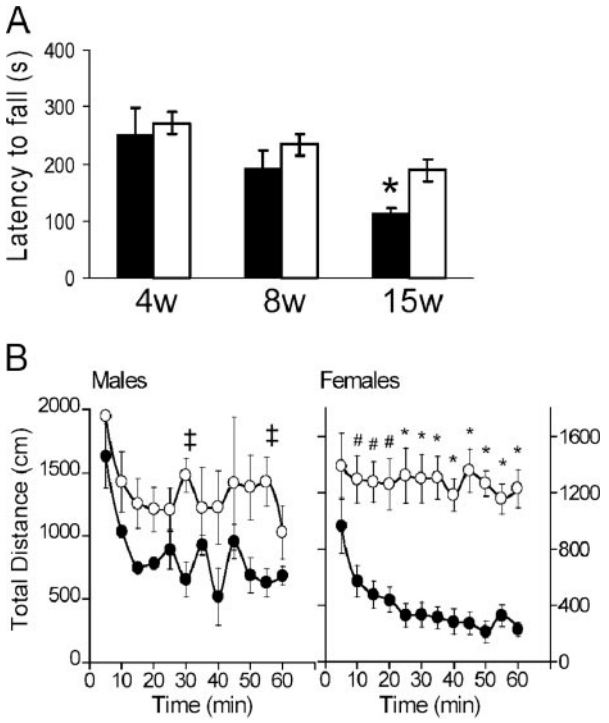

FIG. 3. Unconventional performance of shaking KO mice on rotarod, accompanied by marked hyperactivity. Mice at 4, 8, and 15 weeks (w) of age were challenged on an accelerating rotarod (five mice for each genotype). (A) KO mice (open bars) performed better than WT mice (filled bars) on the rotarod with a longer average time from latency to fall, and this difference was significant at 15 weeks of age (*, $P < 0.007$). (B) KO mice also display hyperactive locomotor activity. Data for male and female mice between 8 and 10 weeks of age (12 mice for each sex and genotype) are shown. Total distance traveled per 5-min sample over 60 min is shown for WT (closed circles) and KO (open circles) mice. KO female mice exhibited a significant increase in horizontal activity (#, $P < 0.002$; *, $P < 0.0001$), while KO males were less hyperactive (‡, $P < 0.03$).

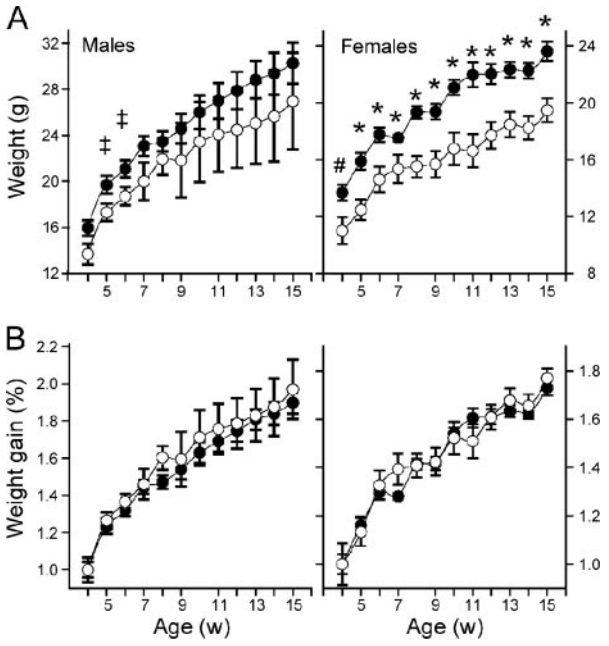

FIG. 4. The body weights of KO mice are significantly reduced, but growth rates are similar to those of WT mice. (A) In male and female mice aged 4 to 15 weeks (w), *Abca2* KO mice (open circles) have significantly lower body weight than WT counterparts (filled circles), a phenotype more pronounced in females (#, $P < 0.03$; *, $P < 0.009$) than males (‡, $P < 0.05$). (B) However, the growth rates of both sexes are similar to those of WT mice during this period.

more rapidly on the beam, often resulting in a fall (see video S2 in the supplemental material).

Improved rotarod performance and hyperactivity of KO mice. Although the shaking and nervous disposition of the KO mice inhibited their ability to counterbalance on a metal beam (see video S2 in the supplemental material), the KO animals performed better than the WT animals when challenged on the rotarod apparatus at 4, 8, and 15 weeks of age (Fig. 3A). This difference in the time from latency to fall from the apparatus was significant at 15 weeks (WT versus KO; $P < 0.007$). Interestingly, the decline with age in the time from latency to fall seen in WT animals (8 weeks versus 15 weeks; $P = 0.045$) does not occur in the KO cohorts ($P = 0.16$). Initially, KO animals in their home cages (see videos S3 and S4 in the supplemental material) displayed heightened activity and rearing behavior compared to their WT littermates (see videos S5 and S6 in the supplemental material). In order to quantify these movements, we utilized Digiscan locomotor recording devices to measure horizontal and vertical activity over a habituation period (within 60 min for WT animals). Both male and female WT mice display this habituation by a decline in total distance traveled (Fig. 3B) with a concomitant decrease in vertical activity (data not shown). Male KO mice have only slightly higher activity than WT males, which reached significance at the 30- and 55-min time points ($P < 0.05$). Female KO mice showed significant hyperactivity compared to their WT counterparts from 10 to 60 min (P was <0.002 through 20 min and <0.0001 from 25 to 60 min). These data indicated that KO mice, particularly females, display an inability to habituate to the novel environment by 60 min.

KO mice have a reduced body weight but similar growth rate compared to WT littermates. A significantly lower body weight in KO mice compared to WT littermates was observed in both males (at 5 and 6 weeks of age) and females (from 4 to 14 weeks of age) (Fig. 4A). Growth rates during this period were similar (Fig. 4B). The difference in weight cannot be attributed to differences in the amount of food consumed per animal (approximately 30 g/week for males, 25 g/week for females) in both KO and WT mice. Females retain a significantly lower weight at the full-grown age of 14 weeks, indicating a long-term difference in development and/or metabolism.

Plasma cholesterol and CNS tissue lipid composition unaffected by ABCA2 deficiency. Total, esterified, and free plasma cholesterol levels were similar in the KO, HET, and WT littermates ($P > 0.10$; $n = 4$) (Table 3). In addition, HDL levels were similar; indicating that, unlike in *Abca1* KO mice (29), the loss of ABCA2 expression does not impact levels of circulating HDL.

Concentration of ceramide, sphingosine, and sphingomyelin species determined by liquid chromatography/mass spectrometry analysis (see Materials and Methods) did not differ signif-

TABLE 3. Plasma cholesterol levels in KO mice compared to WT littermates

Genotype	Amt of indicated cholesterol in plasma (mg/dl)[a]			
	TC	HDL	FC	EC
WT	164 ± 15	91 ± 16	41 ± 1	115 ± 5
KO	159 ± 9	81 ± 13	42 ± 1	106 ± 10

[a] Data are reported as means ± standard deviations. Abbreviations: TC, total cholesterol; FC, free cholesterol; EC, esterified cholesterol.

icantly between WT and KO littermates (P was >0.4 for all species).

CNS and peripheral nervous system tissue appear normal at the histological level. Brain, spinal cord, and sciatic nerve samples were harvested from WT and KO littermates at 6 weeks of age. Hematoxylin and eosin- and LFB-stained sections showed that KO tissues were indistinguishable from those of WT littermates at the light microscopic level.

Expression of myelin proteins in CNS tissues. Since the shaking phenotype observed in the *Abca2* KO mouse is reminiscent of several models of genetic myelinopathy (31, 35, 37), we examined the expression of crucial myelin proteins (myelin basic protein [MBP], proteolipid protein [PLP], and 2′,3′-cyclic nucleotide 3′-phosphodiesterase [CNPase]) using RT- and real-time PCR. An approximate 20 to 30% reduction in MBP, PLP, and CNPase transcripts were observed in cerebellum and cerebrum samples from KO mice (Fig. 5A). While these values fell short of statistical significance (Fig. 5A) (P values were 0.07, 0.09, and 0.25, respectively, for cerebellum, and 0.057, 0.50, and 0.18, respectively, for cerebrum), this trend was reversed in KO mouse spinal cord, where levels of these genes met or exceeded that of WT animals (Fig. 5A) (P values were 0.04, 0.18, and 0.53, for MBP, PLP, and CNP, respectively). Loss of ABCA2 caused an induction of MBP and PLP transcription in KO mouse spinal cord but not KO mouse cerebrum, consistent with the myelin thickness data described below.

Ultrastructural analysis showed that KO mice have reduced compaction of myelin sheath in cerebrum and spinal cord. The morphology and ultrastructure of myelin sheath were examined in TEM images of cerebrum, cerebellum, and spinal cord (Table 4). Myelin-related gene expression in cerebrum (unchanged or slightly decreased) and spinal cord (increased) appears to correlate with the thickness of myelin sheath surrounding axons in these tissues (P values were 0.02 for cerebrum and <0.016 for spinal cord) (Table 4; Fig. 5). In cerebrum, a greater percentage of axons in KO (24.1%) than in WT (12.8%) mice fell within the smallest size range of myelin thickness (<0.05 to 0.06 μm) (Fig. 5B). A greater proportion of WT cerebral axons (8.5% and 7.5%) were represented in the higher size ranges (0.16 to 0.20 μm and >0.21 μm, respectively), while those of KO mice were reduced or absent (5% and 0%). Conversely, in spinal cord, more WT axons had sheath measurements in the smaller size ranges (34.4% WT versus 23.2% KO in the <0.15 μm group), while KO axons were predominant in the higher ranges (13.6% and 10.6% in the 0.65- to 0.94-μm and >0.95-μm groups, respectively, versus 4.5% and 1.4% for WT) (Fig. 5B). Myelin ultrastructure in females also shows a significant increase in KO sheath thickness in spinal cord (0.20 ±0.14) compared to WT (0.12 ±0.07; $P < 0.0001$). Although the myelin sheath thickness differed in KO cerebrum (hypomyelination) and spinal cord (hypermyelination), both of these tissues showed a reduction in periodicity/myelin compaction (P values were <0.0001 and 0.0006, respectively) (Table 4). Ultrastructure of myelin sheath was unchanged in micrographs of cerebellum. Taken together, these data suggest an inability to correctly compact myelin in spinal cord and cerebrum, an ultrastructural abnormality that may account for faulty nerve conduction and a resulting tremor.

DISCUSSION

Gene-targeted disruption of ABCA2 in mice resulted in global loss of mRNA/protein expression, a shaking phenotype concomitant with reduced myelin compaction, and differences in myelin thickness in cerebrum and spinal cord. Reduced body weight and hyperactivity were developmental/behavioral defects more prevalent in KO females than males. The changes in myelin ultrastructure in KO CNS tissue are abnormalities that may cause faulty nerve conduction and a resulting tremor.

Impact of *Abca2* null genotype on CNS myelin. The reduced periodicity of myelin in cerebrum and spinal cord suggests a defect in membrane packing, an event occurring during late-stage oligodendrocyte differentiation. Proper redistribution of PLP and MBP to the myelin sheath and aggregation of ion channels at the nodes of Ranvier are critical during this phase of oligodendrocyte maturation (3). Since ABCA2 has been proposed to be concomitantly up-regulated with myelination in oligodendrocytes (38), the transporter may serve as a regulator of cholesterol and/or phospholipid flux to the myelin membrane. Even though the total concentrations of membrane lipids (ceramide, sphingosine, and sphingomyelin) were not altered in the CNS of KO animals, the local concentrations within the myelin membrane and lipid rafts remain unknown. Whether reduced packing of myelin sheath in KO spinal cord and cerebrum is a result of altered membrane composition (and improper localization of protein constituents), mechanical membrane wrapping, and/or availability of cholesterol and phospholipids is a subject for future study.

Tremor has been reported in several mouse models of myelinopathy, including mutants for MBP, PLP, and CNP (13, 24, 31, 35). Each of these proteins plays a role in the establishment and maintenance of myelin membrane; therefore, we examined their expression in CNS tissue of *Abca2* KO mice. Expression of these myelin-related genes was slightly decreased in both cerebrum and cerebellum of KO animals. However, significantly higher levels of MBP mRNA were observed in spinal cord, suggesting transcriptional overcompensation, perhaps representing a futile effort to properly compact the membrane layers. It is also likely that the KO spinal cord contains more MBP transcript due to the presence of thick layers of myelin membrane.

Slack, noncompact spinal cord and cerebral myelin observed in *Abca2* KO mice is an ultrastructural pathology that can result in a physical tremor from faulty nerve conduction. However, the behavioral changes (hyperactivity, lack of habituation) may also result from altered neurotransmission. Mice deficient in neuronal low-density lipoprotein receptor-related

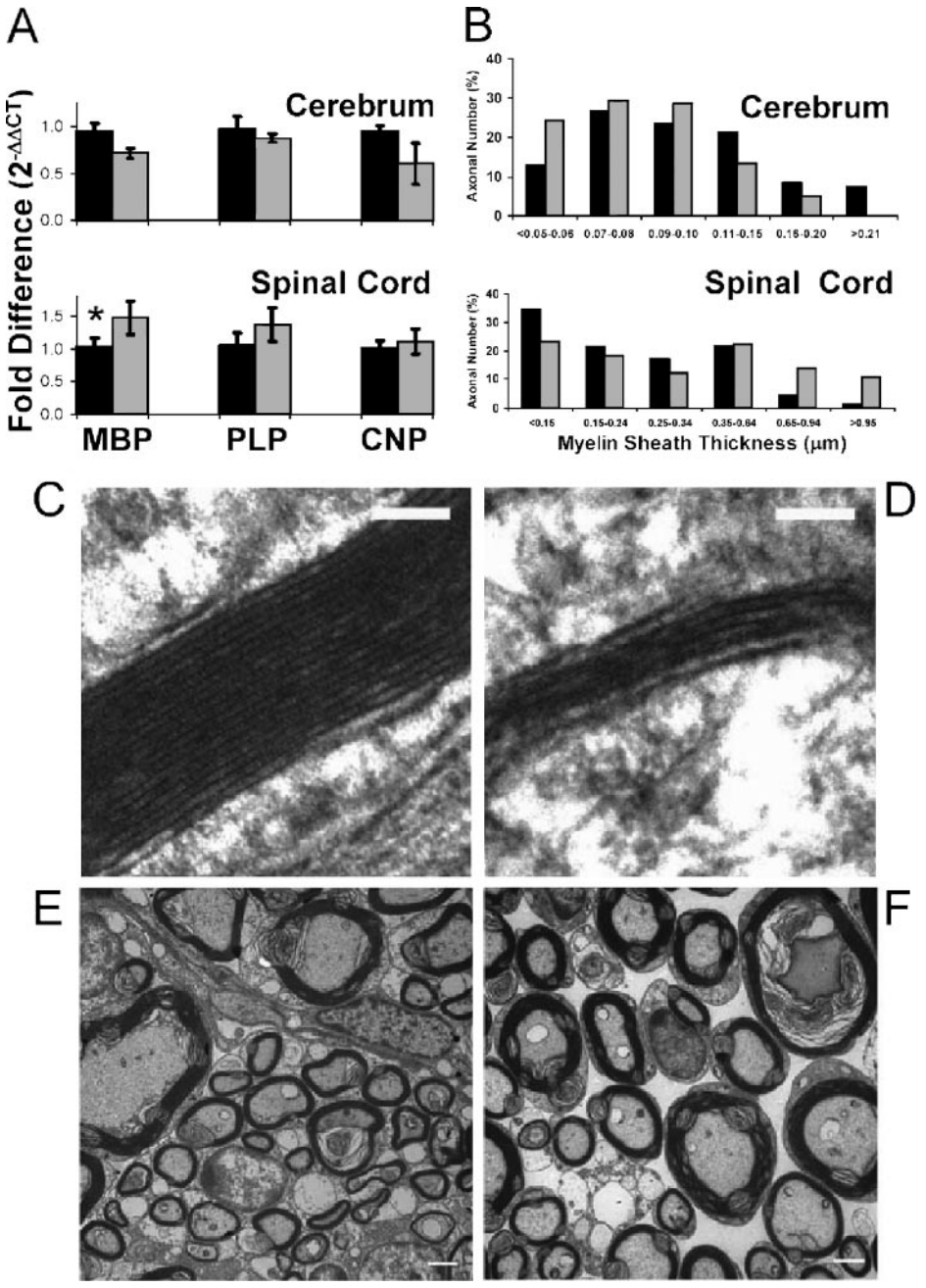

FIG. 5. Reduced myelin compaction in spinal cord and cerebrum of KO mice, accompanied by differences in sheath thickness. (A) Expression of the myelin-associated gene products MBP, PLP, and CNP was determined by real-time PCR for cerebrum and spinal cord in WT (black bars) and KO (gray bars) mice. An increase in MBP and PLP expression in KO spinal cord was observed (*, $P = 0.04$); however, PLP levels fell short of significance due to variation among the samples ($P = 0.18$). CNP levels in both cerebrum and spinal cord were unchanged (P values were 0.18 and 0.53, respectively). The levels of MBP, PLP, and CNP in KO cerebrum did not differ significantly from those of WT cerebrum. Similar relative levels were also shown in cerebellum (data not shown). (B) Histogram showing the percentage of myelin sheaths measured in WT (black bars) compared to KO (gray bars) mice. Percentage of axons categorized into size (thickness) bins from smallest (left) to largest (right) in cerebrum and spinal cord (Table 4). Representative TEM images of myelin sheath cross sections in cerebrum (C and D [scale bar, 100 nm]) and spinal cord (E and F [scale bar, 2 μm]) from WT (C and E) or KO (D and F) mice.

protein 1 (LRP1) also display hyperactivity and tremor (28), a phenotype attributed to neurotransmitter-related postsynaptic response functions of this protein. Aberrant synaptic plasticity is associated with a wide range of neurological diseases including Parkinson's disease (25) and Alzheimer's disease (32). Our preliminary data show that ABCA2 cofractionates with synaptic vesicle markers (unpublished). This observation is concordant with the localization of the transporter in GABAergic and glutamatergic neurons and a proposed role of ABCA2 in regulating the availability of cholesterol for synaptic vesicles (2).

TABLE 4. Effects of *Abca2* null genotype on CNS myelin ultrastructure

Tissue	Periodicity (major dense lines/μm)[a]		*P* value	Thickness (μm)[a]		*P* value
	WT	KO		WT	KO	
Cerebellum	77.7 ± 4.4	77.1 ± 4.2	0.73	0.15 ± 0.07	0.14 ± 0.06	0.17
Cerebrum	73.4 ± 6.6	62.4 ± 8.0	<0.0001	0.11 ± 0.05	0.09 ± 0.03	0.0008
Spinal cord	72.1 ± 6.4	66.1 ± 5.7	0.0006	0.27 ± 0.21	0.42 ± 0.33	<0.0001

[a] Data are reported as means ± standard deviations.

Taken together, the hyperactivity and tremor may be caused by a combination of deleterious effects in the CNS, including altered neurotransmission and myelin defects.

Altered morphology within motor coordination centers in cerebellum is a common pathology associated with tremor (14). As demonstrated by their rotarod performance, *Abca2* KO animals lack the prototypical ataxia observed in other neurological models (10, 34). This is consistent with a lack of overt myelin defects in the cerebellum (Table 4). In addition, the improved rotarod performance, especially in 15-week-old KO mice, may be a result of the hyperactive nature and smaller average body size (i.e., facilitating ease of movement on the small rod) in these animals.

Sexual disparities in body weight and hyperactivity in KO mice. Decreased body weight among KO mice was also more pronounced in females than in males. This difference was not a factor of food consumption but may be developmental or metabolic in nature, as the average weight of KO females, over time, did not supercede that of WT. Consistent with altered nutrient metabolism is the observation of increased numbers of mitochondria in sciatic nerve TEM images (unpublished data). Embryonic lethality among male KO mice may underlie the phenotypic disparity between the sexes, such that the most severe phenotypes could be observed in surviving females, excluding that of males.

The observation that hyperactivity and reduced body weight were more pronounced in female KO mice suggests a sex-dependent (and perhaps estradiol-dependent) impact of ABCA2 loss. Dysregulation of cholesterol homeostasis and/or hormonal signaling are associated with several human pathologies, including atherosclerosis and AD (4, 12, 17, 30, 45). High plasma cholesterol and depletion of 17β estradiol in postmenopausal females are correlated to development of AD and heart disease (8, 21). Treatment with either statins or estrogen-based therapeutics has shown promising decreases in AD incidence (8, 45). Although the mechanism of estrogen-dependent neuroprotection is unknown, a nonreceptor-based pathway involving antioxidant scavenging of reactive oxygen species by 17β-estradiol has been proposed (8). Previously, we showed that ABCA2 expression enhances resistance to reactive oxygen species, estradiol, and estramustine. Further, hormone-based treatment (using estradiol, estramustine, and progesterone) caused up-regulation of ABCA2 expression. Given the current sexual disparity in the response to ABCA2 loss of function, we propose that the gender-based protection of estradiol against neurodegeneration may be mediated by ABCA2.

Putative role of ABCA2 in cholesterol trafficking. Oligodendrocytes and Schwann cells both require substantial quantities of membrane constituents for the formation of myelin sheath and may be particularly susceptible to mistrafficking of cholesterol. Niemann-Pick disease type C (NPC) is a lysosomal storage disease caused by mutations in either NPC1 or NPC2, both of which are required for the efflux of cholesterol from lysosomes. Neurodegeneration resulting from the intracellular accumulation of sphingolipids and cholesterol is characteristic of NPC (27). In the *NPC* knockout mouse, hypomyelination occurs in the cerebral cortex and the corpus callosum, accounting for the tremor and ataxia observed in these mice (39). High expression of ABCA2 was shown in NPC1 fibroblasts (6), indicating potential cross talk between the two proteins. However, in *Abca2* KO animals, the levels of NPC1 mRNA were similar to WT levels in KO liver and brain tissues, indicating that expression of ABCA2 and NPC1 are not inversely correlated. Similar shaking phenotypes exist among *Abca2*, *NPC*, and other genetic KO models relating to cholesterol synthesis (34) and trafficking (46). Together, these animal models may help clarify the impact of cholesterol dysregulation on human neurodegeneration.

We examined cholesterol levels in *Abca2* KO mice due to the close homology of ABCA2 with the HDL-forming ABCA1 transporter and the fact that both A1 and A2 and elevated plasma cholesterol are associated with AD (26, 44). Plasma HDL and free cholesterol levels were similar in KO and WT mice, implying that circulating cholesterol levels are independent of ABCA2. As previously suggested (6), this transporter may participate in, but is not required for, feedback pathways in de novo cholesterol synthesis and uptake. Our data also show that compensatory up-regulation of murine ABCA subfamily members (A1, A3, A5, and A7) does not occur in the absence of ABCA2.

Implications of ABCA2 association with hormones and neurodegenerative disease. The *Abca2* KO genotype had a negative impact on the compaction of myelin membrane, a late-stage event in oligodendrocyte differentiation. This is consistent with a previous study showing that potential transcription factor binding sites, associated with neural and myeloid differentiation, lie within the ABCA2 promoter (19). Further, up-regulation of this transporter occurs during differentiation of monocytes into macrophages (19). ABCA2 expression has also been found in regions of the brain associated with adult neurogenesis (2). Putative sterol ring-containing substrates of ABCA2 transport include cholesterol, 17β estradiol, estramustine (an estradiol derivative), and progesterone (1, 16, 18, 23, 41). ABCA2 may serve to transport and/or localize these small hydrophobic substrates into vesicles or membrane microdomains for lateral transport or eventual fusion with a membrane destination (plasma membrane in macrophages, myelin membrane in oligodendrocytes, or synaptic vesicles in neurons), impacting differentiation and nerve function.

We report a skittish *Abca2* knockout mouse line with a shaking, small, and hyperactive phenotype. Reduced membrane compaction and differences in the thickness of myelin layers in KO spinal cord and cerebrum are likely the causes of the observed tremor. The severity of the KO phenotype among females further supports a role of ABCA2 in the regulation/trafficking of steroid hormones and preservation of normal CNS structure/function. Further studies will help uncover the developmental and behavioral impact of ABCA2 loss of function and contribute to the growing body of literature linking transporter function to neurodegenerative disease.

ACKNOWLEDGMENTS

We thank Peter Kalivas and Alejandra Pacchioni (MUSC Department of Neurosciences) for helpful discussion and equipment for behavioral assays, Mostafa Fraig and Cynthia Welsh (MUSC Pathology & Laboratory Medicine) for pathological expertise, and Roderick Bronson (Harvard Medical School Rodent Histopathology Core) for additional pathological analysis of CNS tissues.

This work was supported by the National Institutes of Health/National Cancer Institute, grant CA083778-06. J.T.M. is a postdoctoral fellow supported by NIH Ruth L. Kirschstein National Research Service award CA117749.

REFERENCES

1. **Boonstra, R., H. Timmer-Bosscha, J. van Echten-Arends, D. M. van der Kolk, A. van den Berg, B. de Jong, K. D. Tew, S. Poppema, and E. G. de Vries.** 2004. Mitoxantrone resistance in a small cell lung cancer cell line is associated with ABCA2 upregulation. Br. J. Cancer **90**:2411–2417.
2. **Broccardo, C., V. Nieoullon, R. Amin, F. Masmejean, S. Carta, S. Tassi, M. Pophillat, A. Rubartelli, M. Pierres, G. Rougon, A. Nieoullon, G. Chazal, and G. Chimini.** 2006. ABCA2 is a marker of neural progenitors and neuronal subsets in the adult rodent brain. J. Neurochem. **97:**345–355.
3. **Butt, A. M., and M. Berry.** 2000. Oligodendrocytes and the control of myelination in vivo: new insights from the rat anterior medullary velum. J. Neurosci. Res. **59:**477–488.
4. **Chen, Y., and M. Hughes-Fulford.** 2001. Human prostate cancer cells lack feedback regulation of low-density lipoprotein receptor and its regulator, SREBP2. Int. J. Cancer **91:**41–45.
5. **Chen, Z. J., B. Vulevic, K. E. Ile, A. Soulika, W. Davis, Jr., P. B. Reiner, B. P. Connop, P. Nathwani, J. Q. Trojanowski, and K. D. Tew.** 2004. Association of ABCA2 expression with determinants of Alzheimer's disease. FASEB J. **18:**1129–1131.
6. **Davis, W., Jr., J. T. Boyd, K. E. Ile, and K. D. Tew.** 2004. Human ATP-binding cassette transporter-2 (ABCA2) positively regulates low-density lipoprotein receptor expression and negatively regulates cholesterol esterification in Chinese hamster ovary cells. Biochim. Biophys. Acta **1683:**89–100.
7. **Dean, M.** 2005. The genetics of ATP-binding cassette transporters. Methods Enzymol. **400:**409–429.
8. **Dhandapani, K. M., and D. W. Brann.** 2002. Protective effects of estrogen and selective estrogen receptor modulators in the brain. Biol. Reprod. **67:** 1379–1385.
9. **Efferth, T., J. P. Gillet, A. Sauerbrey, F. Zintl, V. Bertholet, F. de Longueville, J. Remacle, and D. Steinbach.** 2006. Expression profiling of ATP-binding cassette transporters in childhood T-cell acute lymphoblastic leukemia. Mol. Cancer Ther. **5:**1986–1994.
10. **Fewou, S. N., H. Bussow, N. Schaeren-Wiemers, M. T. Vanier, W. B. Macklin, V. Gieselmann, and M. Eckhardt.** 2005. Reversal of non-hydroxy:alpha-hydroxy galactosylceramide ratio and unstable myelin in transgenic mice overexpressing UDP-galactose:ceramide galactosyltransferase. J. Neurochem. **94:**469–481.
11. **Fitzgerald, M. L., K.-I. Okuhira, G. F. Short III, J. J. Manning, S. A. Bell, and M. W. Freeman.** 2004. ATP-binding cassette transporter A1 contains a novel C-terminal VFVNFA motif that is required for its cholesterol efflux and ApoA-I binding activities. J. Biol. Chem. **279:**48477–48485.
12. **Freeman, M. R., and K. R. Solomon.** 2004. Cholesterol and prostate cancer. J. Cell. Biochem. **91:**54–69.
13. **Griffiths, I., M. Klugmann, T. Anderson, D. Yool, C. Thomson, M. H. Schwab, A. Schneider, F. Zimmermann, M. McCulloch, N. Nadon, and K. A. Nave.** 1998. Axonal swellings and degeneration in mice lacking the major proteolipid of myelin. Science **280:**1610–1613.
14. **Grusser-Cornehls, U., and J. Baurle.** 2001. Mutant mice as a model for cerebellar ataxia. Prog. Neurobiol. **63:**489–540.
15. **Halliwell, B.** 2001. Role of free radicals in the neurodegenerative diseases: therapeutic implications for antioxidant treatment. Drugs Aging **18:**685–716.
16. **Hazlehurst, L. A., S. A. Enkemann, C. A. Beam, R. F. Argilagos, J. Painter, K. H. Shain, S. Saporta, D. Boulware, L. Moscinski, M. Alsina, and W. S. Dalton.** 2003. Genotypic and phenotypic comparisons of de novo and acquired melphalan resistance in an isogenic multiple myeloma cell line model. Cancer Res. **63:**7900–7906.
17. **Hughes-Fulford, M., Y. Chen, and R. R. Tjandrawinata.** 2001. Fatty acid regulates gene expression and growth of human prostate cancer PC-3 cells. Carcinogenesis **22:**701–707.
18. **Ile, K. E., W. Davis, Jr., J. T. Boyd, A. M. Soulika, and K. D. Tew.** 2004. Identification of a novel first exon of the human ABCA2 transporter gene encoding a unique N-terminus. Biochim. Biophys. Acta **1678:**22–32.
19. **Kaminski, W. E., A. Piehler, K. Pullmann, M. Porsch-Ozcurumez, C. Duong, G. M. Bared, C. Buchler, and G. Schmitz.** 2001. Complete coding sequence, promoter region, and genomic structure of the human ABCA2 gene and evidence for sterol-dependent regulation in macrophages. Biochem. Biophys. Res. Commun. **281:**249–258.
20. **Kim, W. S., G. J. Guillemin, E. N. Glaros, C. K. Lim, and B. Garner.** 2006. Quantitation of ATP-binding cassette subfamily-A transporter gene expression in primary human brain cells. Neuroreport **17:**891–896.
21. **Kivipelto, M., E. L. Helkala, M. P. Laakso, T. Hanninen, M. Hallikainen, K. Alhainen, H. Soininen, J. Tuomilehto, and A. Nissinen.** 2001. Midlife vascular risk factors and Alzheimer's disease in later life: longitudinal, population based study. BMJ **322:**1447–1451.
22. **Kuhn, P. L., E. Petroulakis, G. A. Zazanis, and R. D. McKinnon.** 1995. Motor function analysis of myelin mutant mice using a rotarod. Int. J. Dev. Neurosci. **13:**715–722.
23. **Laing, N. M., M. G. Belinsky, G. D. Kruh, D. W. Bell, J. T. Boyd, L. Barone, J. R. Testa, and K. D. Tew.** 1998. Amplification of the ATP-binding cassette 2 transporter gene is functionally linked with enhanced efflux of estramustine in ovarian carcinoma cells. Cancer Res. **58:**1332–1337.
24. **Lappe-Siefke, C., S. Goebbels, M. Gravel, E. Nicksch, J. Lee, P. E. Braun, I. R. Griffiths, and K. A. Nave.** 2003. Disruption of Cnp1 uncouples oligodendroglial functions in axonal support and myelination. Nat. Genet. **33:** 366–374.
25. **Lotharius, J., and P. Brundin.** 2002. Impaired dopamine storage resulting from alpha-synuclein mutations may contribute to the pathogenesis of Parkinson's disease. Hum. Mol. Genet. **11:**2395–2407.
26. **Mace, S., E. Cousin, S. Ricard, E. Genin, E. Spanakis, C. Lafargue-Soubigou, B. Genin, R. Fournel, S. Roche, G. Haussy, F. Massey, S. Soubigou, G. Brefort, P. Benoit, A. Brice, D. Campion, M. Hollis, L. Pradier, J. Benavides, and J. F. Deleuze.** 2005. ABCA2 is a strong genetic risk factor for early-onset Alzheimer's disease. Neurobiol. Dis. **18:**119–125.
27. **Maxfield, F. R., and I. Tabas.** 2005. Role of cholesterol and lipid organization in disease. Nature **438:**612–621.
28. **May, P., A. Rohlmann, H. H. Bock, K. Zurhove, J. D. Marth, E. D. Schomburg, J. L. Noebels, U. Beffert, J. D. Sweatt, E. J. Weeber, and J. Herz.** 2004. Neuronal LRP1 functionally associates with postsynaptic proteins and is required for normal motor function in mice. Mol. Cell. Biol. **24:**8872–8883.
29. **McNeish, J., R. J. Aiello, D. Guyot, T. Turi, C. Gabel, C. Aldinger, K. L. Hoppe, M. L. Roach, L. J. Royer, J. de Wet, C. Broccardo, G. Chimini, and O. L. Francone.** 2000. High density lipoprotein deficiency and foam cell accumulation in mice with targeted disruption of ATP-binding cassette transporter-1. Proc. Natl. Acad. Sci. USA **97:**4245–4250.
30. **Molony, T.** 2003. Use of cholesterol drugs may decrease breast cancer risk. J. Dent. Hyg. **77:**214.
31. **Rosenbluth, J.** 1980. Central myelin in the mouse mutant shiverer. J. Comp. Neurol. **194:**639–648.
32. **Rowan, M. J., I. Klyubin, Q. Wang, and R. Anwyl.** 2005. Synaptic plasticity disruption by amyloid beta protein: modulation by potential Alzheimer's disease modifying therapies. Biochem. Soc. Trans. **33:**563–567.
33. **Rozen, S., and H. Skaletsky.** 2000. Primer3 on the WWW for general users and for biologist programmers. Methods Mol. Biol. **132:**365–386.
34. **Saher, G., B. Brugger, C. Lappe-Siefke, W. Mobius, R. Tozawa, M. C. Wehr, F. Wieland, S. Ishibashi, and K. A. Nave.** 2005. High cholesterol level is essential for myelin membrane growth. Nat. Neurosci. **8:**468–475.
35. **Sidman, R. L., M. M. Dickie, and S. H. Appel.** 1964. Mutant mice (quaking and jimpy) with deficient myelination in the central nervous system. Science **144:**309–311.
36. **Standridge, J. B.** 2006. Vicious cycles within the neuropathophysiologic mechanisms of Alzheimer's disease. Curr. Alzheimer Res. **3:**95–108.
37. **Suter, U., A. A. Welcher, T. Ozcelik, G. J. Snipes, B. Kosaras, U. Francke, S. Billings-Gagliardi, R. L. Sidman, and E. M. Shooter.** 1992. Trembler mouse carries a point mutation in a myelin gene. Nature **356:**241–244.
38. **Tachikawa, M., M. Watanabe, S. Hori, M. Fukaya, S. Ohtsuki, T. Asashima, and T. Terasaki.** 2005. Distinct spatio-temporal expression of ABCA and ABCG transporters in the developing and adult mouse brain. J. Neurochem. **95:**294–304.
39. **Takikita, S., T. Fukuda, I. Mohri, T. Yagi, and K. Suzuki.** 2004. Perturbed myelination process of premyelinating oligodendrocyte in Niemann-Pick type C mouse. J. Neuropathol. Exp. Neurol. **63:**660–673.
40. **Tanzi, R. E., and L. Bertram.** 2001. New frontiers in Alzheimer's disease genetics. Neuron **32:**181–184.
41. **Vulevic, B., Z. Chen, J. T. Boyd, W. Davis, Jr., E. S. Walsh, M. G. Belinsky,**

and K. D. Tew. 2001. Cloning and characterization of human adenosine 5′-triphosphate-binding cassette, sub-family A, transporter 2 (ABCA2). Cancer Res. **61:**3339–3347.
42. **Wang, Y., K. Yamada, Y. Tanaka, K. Ishikawa, and N. Inagaki.** 2005. Expression of ABCA2 protein in human vestibular schwannoma and peripheral nerve. J. Neurol. Sci. **232:**59–63.
43. **Wollmer, M. A., E. Kapaki, M. Hersberger, J. Muntwyler, F. Brunner, M. Tsolaki, H. Akatsu, K. Kosaka, M. Michikawa, D. Molyva, G. P. Paraskevas, D. Lutjohann, A. Eckardstein, C. Hock, R. M. Nitsch, and A. Papassotiropoulos.** 2006. Ethnicity-dependent genetic association of ABCA2 with sporadic Alzheimer's disease. Am. J. Med. Genet. Neuropsychiatr. Genet. **141:**534–536.
44. **Wollmer, M. A., J. R. Streffer, D. Lutjohann, M. Tsolaki, V. Iakovidou, T. Hegi, T. Pasch, H. H. Jung, K. Bergmann, R. M. Nitsch, C. Hock, and A. Papassotiropoulos.** 2003. ABCA1 modulates CSF cholesterol levels and influences the age at onset of Alzheimer's disease. Neurobiol. Aging **24:**421–426.
45. **Wolozin, B., J. Brown III, C. Theisler, and S. Silberman.** 2004. The cellular biochemistry of cholesterol and statins: insights into the pathophysiology and therapy of Alzheimer's disease. CNS Drug Rev. **10:**127–146.
46. **Xie, C., S. D. Turley, P. G. Pentchev, and J. M. Dietschy.** 1999. Cholesterol balance and metabolism in mice with loss of function of Niemann-Pick C protein. Am. J. Physiol. **276:**E336–E344.
47. **Zhou, C., L. Zhao, N. Inagaki, J. Guan, S. Nakajo, T. Hirabayashi, S. Kikuyama, and S. Shioda.** 2001. Atp-binding cassette transporter ABC2/ABCA2 in the rat brain: a novel mammalian lysosome-associated membrane protein and a specific marker for oligodendrocytes but not for myelin sheaths. J. Neurosci. **21:**849–857.
48. **Zhou, C. J., N. Inagaki, S. J. Pleasure, L. X. Zhao, S. Kikuyama, and S. Shioda.** 2002. ATP-binding cassette transporter ABCA2 (ABC2) expression in the developing spinal cord and PNS during myelination. J. Comp. Neurol. **451:**334–345.
49. **Zuker, M.** 2003. Mfold web server for nucleic acid folding and hybridization prediction. Nucleic Acids Res. **31:**3406–3415.